

# Mid-Infrared Silicon-on-Sapphire Polarization Rotator

Joel Guo<sup>1</sup>, Ali Rostamian<sup>1</sup>, Swapnajit Chakravarty<sup>2</sup>, Hai Yan<sup>1</sup>, Chi-Jui Chung<sup>1</sup>, Elham Heidari<sup>1</sup>, Ray Chen<sup>1,2</sup>

<sup>1</sup>Department of Electrical and Computer Engineering, University of Texas at Austin, 10100 Burnet Rd. Austin, TX 78758, USA

<sup>2</sup>Omega Optics, Inc., 8500 Shoal Creek Blvd., Bldg. 4, Suite 200, Austin, Texas 78757, USA

Author e-mail address: [joel.guo@utexas.edu](mailto:joel.guo@utexas.edu), [swapnajit.chakravarty@omegaoptics.com](mailto:swapnajit.chakravarty@omegaoptics.com), [chenr1@austin.utexas.edu](mailto:chenr1@austin.utexas.edu)

**Abstract:** We experimentally demonstrate mid-infrared polarization rotators in silicon-on-sapphire at wavelength  $\lambda = 4.55\mu\text{m}$  to enable integration of quantum cascade lasers and detectors with slotted photonic crystal waveguide gas sensors. Polarization selective grating couplers are also demonstrated. © 2018 The Author(s)

Infrared (IR) spectroscopy is widely accepted as a reliable and low cost technique in sensing applications. However, IR spectroscopy typically requires bulky and expensive optical elements that add additional weight and space constraints in instances where low size, weight and power (SWaP) are desired such as inside airborne platforms and space-crafts. In recent years, quantum cascade laser (QCL) sources have resulted in lasers in mid-infrared wavelengths which probe the fundamental molecular vibrations of most molecules [1, 2]. But, the requirement of a gas cell still makes on-chip integration impossible and heterogeneous integration cumbersome. Multipass gas cells require high finesse mirrors which need to be specially designed for each different wavelength range of operation. External cavity QCLs with gratings are the current method of generating tunable QCLs. However, the system needs mechanical moving parts and requires precision alignment between the source laser and detector, a significant cost impediment in optics and a deployment hassle due to fragile optical alignments.

To address the needs of high sensitivity, we experimentally demonstrated on-chip mid-IR absorption sensors using holey slotted photonic crystal waveguides (HPCWs) [3-6] that have shown feasibility to detect sub-100 parts per billion (ppb) of greenhouse gases such as carbon monoxide [3], chemical warfare simulants such as triethylphosphate [4] and other analytes [5, 6]. The on-chip absorption spectroscopy is based on the enhancement of optical interaction and thus effective reduction of the geometric absorption path length due to slow light effects of a photonic crystal waveguide (PCW) combined with electric field intensity enhancement effects of slot at the middle of the PCW. To address low SWaP requirements, monolithic integration of the HPCWs with QCLs and quantum cascade detectors (QCDs) is required. It is known that the emission from the QCL is transverse magnetic (TM) polarized (electric field perpendicular to plane of propagation). However, photonic crystal waveguides (PCWs) and slotted PCWs have photonic band gaps (PBGs) for transverse electric (TE) polarized propagating light (electric field in the plane of the slab) only. Hence, for integration, it is necessary to incorporate a polarization rotator to rotate polarization from TM to TE (from QCL to passive waveguide section) and back from TE to TM (passive waveguide section to QCD). In addition, waveguide bending loss for TE-polarized modes is in general lower than TM-polarized modes. Polarization rotators have been demonstrated at telecom wavelengths [7, 8]. In this paper, we provide the first experimental demonstration of a polarization rotator in silicon-on-sapphire (SoS) at mid-infrared wavelengths.

The schematic of the polarization rotator is shown in Fig. 1(a). The silicon waveguide geometry is shown in Fig. 1(b). Fig. 1(c) shows the plot of effective index ( $N_{\text{eff}}$ ) versus waveguide width ( $w$ ) of our structure shown in Fig. 1(b) for operation at  $\lambda = 4.55\mu\text{m}$ . As observed from Fig. 1(c), the transition from TM<sub>0</sub> to TE<sub>1</sub> occurs at approximately a waveguide width  $w = 2.55\mu\text{m}$ . The polarization conversion process relies on the conversion of TM<sub>0</sub> to TE<sub>1</sub>, when both modes have the same effective index, by gradually increasing the width of the waveguide (Fig. 1(c)). Once converted to TE<sub>1</sub>, the waveguide is split into 2 single mode waveguide arms, as shown in the lower insets of Fig. 1(a) that propagates TE<sub>0</sub> components at 180-degree phase difference. A phase shift is introduced as shown in one of the arms so that at the input of the 2x2 multimode interference (MMI) device, the TE<sub>0</sub> waves are phase-shifted by 90-degree with respect to each other. An input TM<sub>0</sub> will then be converted to TE<sub>0</sub> that will be observed in the arm 2 as shown in the schematic. The device thus sends an incoming TE<sub>0</sub> wave as TE<sub>0</sub> to arm 1 only with minimum cross-talk in arm 2. For our specific case, we are only interested in TM<sub>0</sub> with output TE<sub>0</sub> to arm 2. In effect, the demonstrated device behaves as a polarization rotator-splitter. Experimentally we validated by choosing polarization selective grating couplers at the input that a TM-polarized input is routed as TE<sub>0</sub> to the upper output arm 2, whilst a TE-polarized input is routed as TE<sub>0</sub> to the lower output arm 1. As observed from Fig. 1(d), 92% conversion efficiency is achieved over a length of 500 $\mu\text{m}$ . The conversion efficiency will be 98% at lengths greater than 2mm. It is also observed that the polarization rotator design is fabrication tolerant as shown by the selection of different widths of the pre-, post- and converter sections around a length of 2mm. Fig. 2 shows 3D finite difference time domain (FDTD) simulation results showing the conversion from TM to TE polarization.

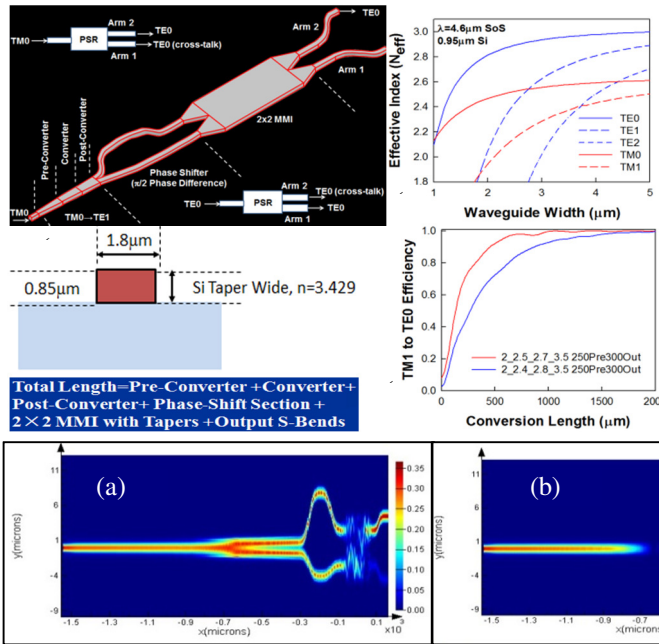


Fig. 1: (a) Schematic of a polarization rotator splitter (b) Effective Index versus width ( $w$ ) of waveguide of the propagating waveguide modes simulated by finite-element modeling (FEM) for the waveguide structure in (c) in silicon-on-sapphire. TM0 to TE1 conversion occurs at  $w \sim 2.55\mu\text{m}$ . The total TM1 to TE1 converter comprises a pre-converter, a converter and post-converter. (d) shows TM0 to TE1 conversion efficiency versus width of the converter section: for the red curve, pre-converter width changes from 2  $\mu\text{m}$  to 2.5  $\mu\text{m}$  over 250  $\mu\text{m}$ , converter width changes from 2.5  $\mu\text{m}$  to 2.7  $\mu\text{m}$  over 1mm, post-converter width changes from 2.7  $\mu\text{m}$  to 3.5  $\mu\text{m}$  over 300  $\mu\text{m}$ . MMI length=117  $\mu\text{m}$ , MMI Width=10  $\mu\text{m}$ ; The phase shifter is formed with waveguides of Bezier curves that gives the required  $\pi/2$  phase shift between the two input arms of the 2x2 MMI. 100% conversion efficiency from TM0 to TE0 is achieved over a total length 2mm.

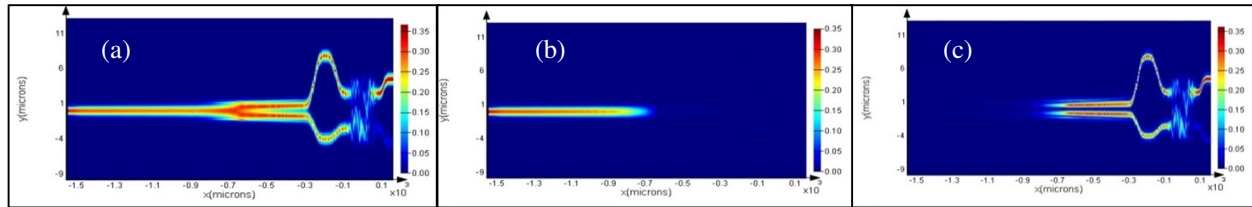


Fig. 2: (a) 3D FDTD simulation showing the electric field intensity magnitude across the complete device with TM0 input on the left side and TE0 output on the right side. (b) shows the electric field intensity magnitude of TM components of the propagating wave. As observed also from (c), complete conversion from TM to TE occurs near the center of the structure. First, TM0 to TE1 conversion after which it splits into two arms.

The light from an external QCL is coupled into the silicon chip using grating couplers via mid-IR optical fibers. Since at the present time, polarization maintaining optical fibers are not available in the mid-IR, it was necessary to design polarization selective grating couplers to efficiently filter the appropriate polarization at the input and output. As observed in Figs. 3 and 4, the designed TE selective grating coupler achieved TE:TM selectivity  $\sim 25:1$  while the designed TM selective grating coupler achieved TE:TM selectivity  $\sim 1:40$ .

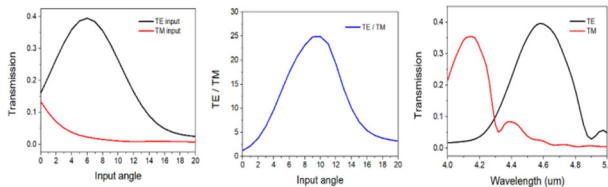


Fig. 3: 2D FDTD simulated transmission for a TE-polarization selective grating coupler versus (a) fiber incident angle and (b) incident wavelength in SoS operating around  $\lambda=4.55\mu\text{m}$

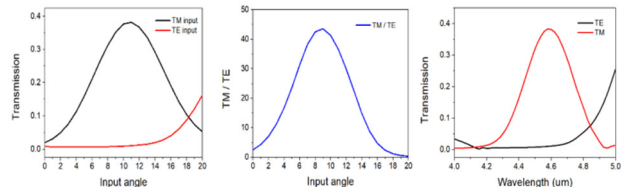


Fig. 4: 2D FDTD simulated transmission for a TM-polarization selective grating coupler versus (a) fiber incident angle and (b) incident wavelength in SoS operating around  $\lambda=4.55\mu\text{m}$

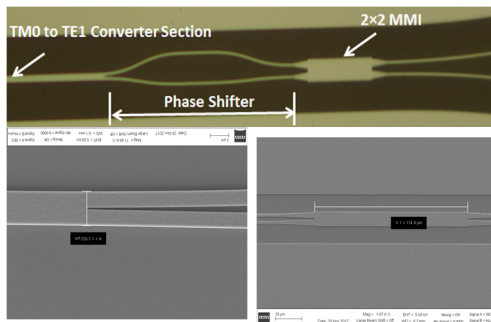


Fig. 5: (a) Microscope image of the polarization rotator. (b) the section where the TE1 mode splits into its two 180-degree shifted TE0 components (The SEM is flipped vertically to match with the microscope image in (a)). (c) Top view SEM images showing (a) the 2x2 multimode interference power splitter section

It was experimentally observed that when the input grating was TE-polarization selective, the splitting ratio between the two output arms was observed on average as 7.6dB, with arm 1 in Fig. 1 having higher output signal than arm 2. When the input grating was TM-polarization selective, the observed splitting ratio between the two arms was -3.65dB with the negative sign

indicating that arm 2 has higher output signal than arm 1. The research was supported by NASA SBIR Contract #NNX17CA44P and NSF Grant # 1711824.

## References

- [1] W. Zhou et al., *Optica* 4(10), 1228 (2017)
- [2] B.G. Lee, et al, *Appl. Phys. Lett.* 91, 231101 (2007)
- [3] CLEO Co-Submission (2018).
- [4] Y. Zou et al., *Sens. and Actuators B: Chemical* 221, 1094 (2015)
- [5] W-C. Lai, et al., *Optics Lett.* 36 (6), 984 (2011).
- [6] W-C. Lai, et al., *Appl. Phys. Lett.* 98 (2), 023304 (2011)
- [7] Y. Ding, H. Ou, C. Peucheret, *Opt. Lett.* 38 (8), 1227 (2013)
- [8] J. Zhang, D-L. Kwong, et al., *Opt. Express* 18 (24), 25624 (2010).